Systems & Control Transactions

Research Article
Foundations of Computer Aided Process Design (FOCAPD 2024)
Breckenridge, Colorado, USA. July 14-18, 2024
Peer Reviewed Conference Proceeding

PSE PRESS

Integration of Chemical Looping Reforming and Shift Reactors for Blue H_2 and N_2 Production

Adrian R. Irhamna[a] and George M. Bollas[a]*

[a] University of Connecticut, Department of Chemical and Biomolecular Engineering, Storrs, CT, USA
* Corresponding Author: george.bollas@uconn.edu.

ABSTRACT

Chemical looping Reforming (CLR) is seen as a promising technology for blue hydrogen production. With proper control, CLR in fixed bed reactors has demonstrated the capability to generate blue hydrogen and nitrogen from a single reactor. To enhance efficiency and H_2 purity in the product stream, integration of a CLR reactor with a heat recovery system and a Shift reactor is essential. This study explores the design and control of an integrated CLR-Shift reactors system. The integrated system yields a product stream with 75% H_2 mole fraction during the Reforming step of CLR, and a nitrogen with high purity (98%) during the Oxidation step. In the best-case scenario, the integrated system produces H_2 and N_2 at a molar ratio of 1.26 with H_2 production efficiency of 80.1%.

Keywords: Chemical-looping reforming, shift reactor, optimal control problem, blue hydrogen and nitrogen production.

INTRODUCTION

The imperative of decarbonization makes hydrogen one of the top candidates to address the need for future energy carriers. Currently, 95% of hydrogen comes from fossil fuels through conventional steam methane reforming, resulting in emissions of over 12 kg of CO_2 per kg of H_2 [1]. This hydrogen production route is known as grey hydrogen. **Figure 1** provides a visual representation of the hydrogen color spectrum, classifying hydrogen based on production techniques, byproducts, feedstock, and energy source. Green hydrogen, generated through water electrolysis powered by renewable energy sources, is regarded as the most environmentally friendly method of hydrogen production. Despite its environmental advantages, the current cost of green hydrogen is nearly four times that of grey hydrogen [2], posing economic challenges for its utilization. Blue hydrogen emerges as a promising alternative. While it still originates from hydrocarbons, this process requires capturing CO_2, minimizing its release to the atmosphere. This approach allows for the utilization of established hydrogen production technologies, such as steam methane reforming, with the addition of a CO_2 capture process in the plant. Blue hydrogen is considered a cost-effective solution during this transitional phase until green hydrogen becomes more economically competitive.

The increase in hydrogen production requires a suitable carrier for large-scale transport and storage. A hydrogen carrier becomes imperative to tackle the inherent challenge of hydrogen's low density. Ammonia is considered as a potential candidate for a hydrogen carrier, offering the ability to store larger quantities of hydrogen in a smaller volume. This route is made possible by capitalizing on the existing global ammonia infrastructure developed for the fertilizer industry [3].

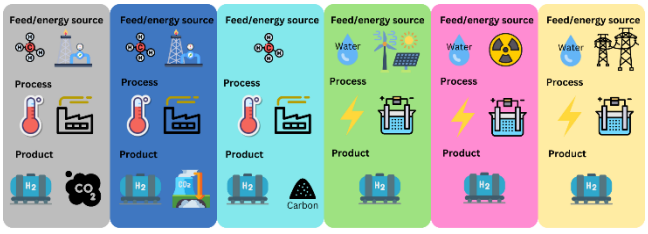

Figure 1. Hydrogen color spectrum

Chemical-looping reforming (CLR) is considered as a promising method for blue hydrogen production [4]. This process relies on the capability of oxygen carriers, performing a cycle of reduction, oxidation, and catalytic

reforming reactions. Opting for a fixed bed reactor in CLR proves more advantageous than a fluidized bed reactor due to its simplicity, prolonged oxygen carrier's lifespan, and the absence of a need for gas-solid separation. However, using fixed bed reactors require a dynamic switching operation to complete the CLR cycle. With proper control, CLR in a fixed bed reactor yields an exit stream with a high H_2 concentration during Reforming step, and a high N_2 concentration during Oxidation step [5]. In our previous research, the optimized CLR reactor produced H_2 with an H_2/CO ratio of 3 during REF and N_2 stream with a purity of 98% during OX [5]. From these results, we identified two key improvements necessary for the CLR reactor. The first enhancement involves the incorporation of a shift reactor to increase the hydrogen concentration in the product stream. The second improvement involves introducing a heat recovery system that utilizes the temperature of the exit gas from CLR as a heat source. This heat recovery system has the potential to substantially improve the overall efficiency of the system.

This study focuses on evaluating the performance of an integrated system comprising a CLR reactor, a shift reactor, and a heat recovery system: a preheater and a steam generator. The main goal is to explore an optimal control strategy for the integrated CLR-Shift reactors system by solving a dynamic optimization problem. The specific objective is to maximize H_2 production while concurrently meeting criteria that guarantee nearly pure N_2 production and ensure the safety and operability of each component within the system. The novelty of this work lies in its integrated approach combining a CLR fixed bed reactor, a heat recovery system, and a shift reactor, facilitating the determination of optimal control parameters and a heat management strategy for highly efficient blue H2 and N2.

PROCESS DESCRIPTION

The integrated system consists of a CLR reactor, a shift reactor, a preheater, and a steam generator, as illustrated in the process flow diagram presented in **Figure 2**. In the CLR reactor, CLR cycle takes place performing oxidation (OX), reduction (REF), and reforming (REF) stages alternately. During OX, the oxygen carrier experiences oxidation by air, generating heat within the reactor and leaving N_2 as the primary product in the exit stream. During RED, the oxygen carrier undergoes reduction of the active metal through a gas-solid reaction with the reducing gas (i.e. CH_4, H_2, CO). The exit stream consists of CO_2 and H_2O, easily separable through condensation for subsequent CO_2 capture and storage. During REF, catalytic reactions occur, resulting in a product stream primarily composed of H_2 and CO. The heat required for both RED and REF comes from the heat generated during OX. The product stream of CLR reactor in each stage is directed to the heat recovery system.

The heat recovery system utilizes the high temperature of the CLR product streams as the heat source. Initially, each hot stream enters the preheater and subsequently progresses to the steam generator. Both the preheater and the steam generator operation are synchronized with the ongoing stage in the CLR reactor. In the preheater, the cold feed gas stream of CLR is heated to the target temperature, around 600 °C. After the preheater, the product stream is used in the steam generator. In the steam generator, the quantity of steam generated in each CLR stage is tuned based on the enthalpy and temperature difference remaining in the hot stream. At the exit of the steam generator, the temperature of the hot stream is set to be around 200 °C.

After the steam generator, the product stream is fed to the Shift reactor. In this reactor, the steam and CO in the product stream undergo conversion to H_2 through the water gas shift reaction. The reactor bed warms up due to the exothermic nature of the water gas shift reaction. During OX and RED, no reactions occur in the Shift reactor, as the stream cool down the reactor bed, keeping it within the active temperature range of 200–350°C.

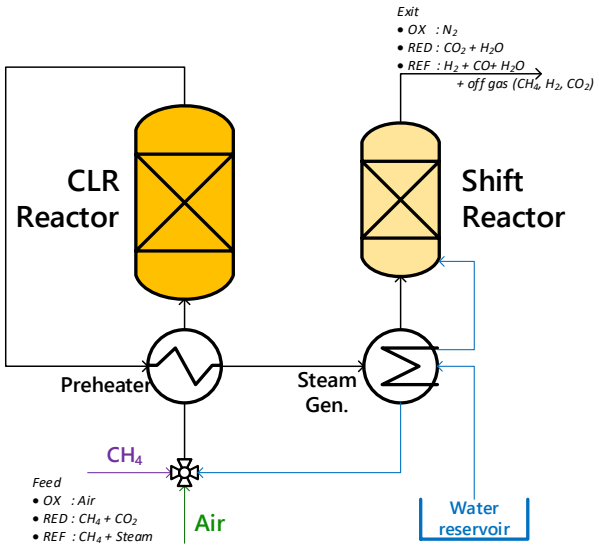

Figure 2. The flow diagram integrated system of the reactor

MODELING

The CLR reactor uses a 1D heterogenous dynamic model of the mass and energy balances for the solid and fluid phases. A summary of the partial differential equations (PDEs) governing the fixed-bed reactor model is presented in **Table 1**. Ni-based oxygen carriers are used in the CLR reactor with reaction kinetics, developed in prior work [6]–[8]. **Table 2** outlines the reactions used in the model, while their corresponding kinetic expressions are provided in [9].

Table 1: Summary of the governing equations of the fixed

bed reactors for CLR and Shift and heat recovery system model of the preheater and the steam generator.

Fixed bed Reactor

Fluid phase

Mass Balance:

$$\epsilon_b \frac{\partial C_i}{\partial t} + \frac{\partial u C_i}{\partial z} = \epsilon_b \frac{\partial}{\partial z}\left(D_{\mathrm{ax},i}\epsilon_b \frac{\partial C_i}{\partial z}\right) + k_{c,i} a_v \left(C_{c,i}|_{Rp} - C_i\right)$$

Energy Balance:

$$\epsilon_b C_{p,f} C_T \frac{\partial T}{\partial t} + C_{p,f} C_T \frac{\partial uT}{\partial z} = \epsilon_b \frac{\partial}{\partial z}\left(\lambda_{\mathrm{ax}} \frac{\partial T}{\partial z}\right) + h_f a_v \left(T_c|_{Rp} - T\right)$$

Momentum Balance:

$$\frac{dP}{dz} = -\left(\frac{1-\epsilon_b}{{\epsilon_b}^3}\right)\left(\frac{\rho {u_o}^2}{D_p}\right)\left(\frac{150}{Re_p} + 1.75\right)$$

Boundary conditions:

$$\epsilon_b D_{\mathrm{ax},i} \left.\frac{\partial C_i}{\partial z}\right|_{z=0} = u_{\mathrm{in}}\left(C_i|_{z=0} - C_{i,\mathrm{in}}\right),$$

$$\epsilon_b \lambda_{\mathrm{ax}} \left.\frac{\partial T}{\partial z}\right|_{z=0} = u_{\mathrm{in}} C_T \left(T|_{z=0} - T_{\mathrm{in}}\right),$$

$$\left.\frac{\partial C_i}{\partial z}\right|_{z=L} = \left.\frac{\partial T}{\partial z}\right|_{z=L} = 0, P|_{z=L} = P_{\mathrm{out}},$$

Solid phase

Mass Balance:

$$\epsilon_c \frac{\partial C_i}{\partial t} + \frac{1}{{r_c}^2}\frac{\partial}{\partial r_c}\left({r_c}^2 J_i\right) = \rho_s \sum R_i$$

Energy Balance:

$$\left((1-\epsilon_c)\rho_s C_{p,s} + \epsilon_c C_{p,c} C_{T,c}\right)\frac{\partial T_c}{\partial t} = \frac{\lambda_s}{{r_c}^2}\frac{\partial}{\partial r}\left({r_c}^2 \frac{\partial T_c}{\partial r_c}\right) + \rho_s \sum (-\Delta H_n)(R_n)$$

Dusty gas model:

$$-\frac{\partial C_{c,i}}{\partial r_c} = \sum_{j=1}^{N} \frac{1}{D_{ij}^e}\left(y_k J_i - y_i J_k\right) + \frac{J_i}{D_{iK}^e}$$

$$J_i|_{r_c=R_p} = k_{c,i}\left(\left.C_{c,i}\right|_{r_c=R_p} - C_i\right),$$

$$-\lambda_s \left.\left(\frac{\partial T_c}{\partial r_c}\right)\right|_{r_c=R_p} = h_f\left(T_c|_{r_c=R_p} - T\right).$$

Heat Recovery System

Streams in each side

$$\dot{Q} = m_c c_{p,c}\left(T_{c,out} - T_{cin}\right) = m_h c_{p,h}\left(T_{h,in} - T_{h,out}\right),$$

Heat exchanger model

$$\dot{Q} = UA\Delta T_{LMTD},\ \Delta T_{LMTD} = \frac{\Delta T_a - \Delta T_b}{\ln\left({\Delta T_a}/{\Delta T_b}\right)},$$

Co-current flow

$$\Delta T_a = T_{h,in} - T_{c,in}, \qquad \Delta T_b = T_{h,out} - T_{c,out},$$

Counter-current flow

$$\Delta T_a = T_{h,in} - T_{c,out}, \qquad \Delta T_b = T_{h,out} - T_{c,in}.$$

Like the CLR reactor, the Shift reactor is modeled using a fixed bed reactor with a 1D heterogenous dynamic model. The corresponding PDEs for the Shift reactor are presented in **Table 1**. Operating at low temperatures (200–350°C), the Shift reactor uses a $Cu/ZnO/Al_2O_3$ catalyst for the water-gas shift reaction. The kinetic correlation for this reaction is adopted from [10], [11] and presented in Eq. (1), where $r_{S,WGS}$ is the reaction rate of the water gas shift reaction, d_{cat} and ε are the diameter and the porosity of the catalyst, respectively, P_S is the pressure in atm, y is the species mole fraction, K_{eq} is the reaction equilibrium described in Eq. (2), R is the gas constant, and T_S is the gas temperature in the Shift reactor in K. The feed of the Shift reactor is the product stream from the CLR reactor, which has been cooled to 200°C.

Table 2: List of feasible reactions in the reduction, reforming, and oxidation using Ni oxygen carriers.

Index	Reactions
(R1)	$H_2 + NiO \rightarrow Ni + H_2O$
(R2)	$CO + NiO \rightarrow Ni + CO_2$
(R3)	$CH_4 + NiO \rightarrow Ni + 2H_2 + CO$
(R4)	$CH_4 + H_2O \leftrightarrow 3H_2 + CO$
(R5)	$CO + H_2O \leftrightarrow H_2 + CO_2$
(R6)	$CH_4 + CO_2 \leftrightarrow 2CO + 2H_2$
(R7)	$CH_4 \leftrightarrow 2H_2 + C$
(R8)	$C + H_2O \leftrightarrow CO + H_2$
(R9)	$C + CO_2 \leftrightarrow 2CO$
(R10)	$O_2 + 2Ni \rightarrow 2NiO$
(R11)	$O_2 + C \rightarrow CO_2$
(R12)	$O_2 + C \rightarrow 2CO$
(R13)	$O_2 + 2CO \rightarrow 2CO_2$

$$r_{S,WGS} = d_{cat}(1-\varepsilon)\, P_S^{(0.5-P_S/250)} \left(2.96 \times 10^5 \frac{\mathrm{mol}}{\mathrm{g.hr}}\right) \exp\left(\frac{-47400\ {}^{\mathrm{J}}/_{\mathrm{mol}}}{RT_S}\right) \times \left(y_{\mathrm{CO}} y_{\mathrm{H_2O}} - \frac{y_{\mathrm{CO_2}} y_{\mathrm{H_2}}}{K_{eq}}\right) \quad (1)$$

$$K_{eq} = \exp\left(\frac{5693.5}{T_S} + 1.077\, ln(T_S) + 5.44 \times 10^{-4} T_S - 1.125 \times 10^{-7} T_S - \frac{49170}{{T_S}^2} - 13.148\right) \quad (2)$$

The energy balance in the preheater and the steam generator are summarized in **Table 1**. The momentum balance, pressure drop, and heat loss in both the preheater and the steam generator were neglected. The models for the CLR and Shift reactors were validated with available experimental data and are illustrated in **Figure 3**.

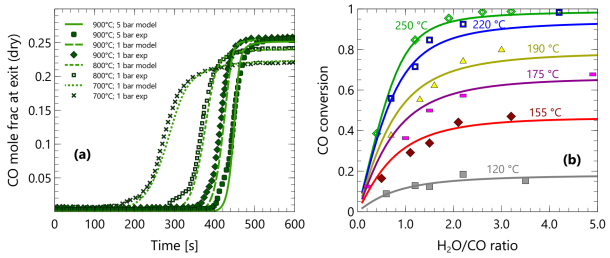

Figure 3. Model validation of CLR (a) and Shift (b) reactors using experimental data reported in [12] and [11] respectively

OPTIMIZATION

The operational challenges associated with a fixed-bed reactor stem mainly from its semi-batch operation. In the fixed bed reactor, the oxygen carrier remains in the reactor while the feed alternates serving CLR stages and complete the cycle. These reactions are kinetically controlled and exhibit different reaction enthalpies. Consequently, the bed temperature and the state of the oxygen carrier experience significant changes during the transition between CLR stages. Each CLR stage produces different gas products, resulting in downstream discontinuities. For H_2 production, the steam-to-methane ratio during REF plays an important role in determining the production of H_2 and in managing carbon deposition. The integration with the heat recovery system and the Shift reactor requires an effective control strategy to ensure the heat generated during OX is appropriately distributed for reactions occurring in the CLR, the heat recovery system, and the Shift reactor. The primary challenge lies in maintaining a high H_2 production while consistently retaining sufficient heat within the integrated system and meeting constraints related to fuel conversion, high N_2 concentration, the energy-temperature difference required for feed gas preheating, steam generation, and the Shift reactor.

To achieve this objective, we formulated an optimal control strategy for the decision variables for the integrated CLR-Shift system. The focus was on maximizing hydrogen production while consistently meeting the dynamic constraints of the system. The decision variables chosen were the time interval of the CLR stages: RED, REF, and OX (τ_{OX}, τ_{RED}, and τ_{REF}), feed gas temperatures, steam-to-methane ratio, the percentage of active metal in oxygen carrier, and the steam added to the Shift reactor, as summarized in **Table 3**. The control profile for the feed gas was modeled using piecewise constant functions, denoted as $\mathbf{u}(\tau_i) = \mathbf{u}$, where $\mathbf{u}$ is the vector of temperature, flow, and composition of the gas stream, while τ_i is the time duration of the i-th CLR step, i.e., OX, RED, and REF. The design vector, $\boldsymbol{\phi}$, summarizes the set of control variables, and was constrained by upper and lower limits defined within the design space, $\boldsymbol{\Phi}$, as presented in Eq. (3).

Table 3: Design variables for the optimal control of the integrated CLR-Shift reactors system

Control variables	Notation
Feed gas temperature Steam-to-methane ratio @REF Methane-to-CO_2 ratio @RED Steam added into the Shift reactor @REF	$\mathbf{u}_i$
Time interval of OX	τ_{OX}
Time interval of RED	τ_{RED}
Time interval of REF	τ_{REF}
Active metal content in OC	ω

The objective function of the optimal control problem is to maximize hydrogen production during the cyclic steady-state operation of the integrated system. The objective function uses a metric called the hydrogen production efficiency, η, shown in Eq. (4), where $F_{S-\text{out},H_2}$ is the hydrogen flowrate at the exit of Shift reactor, $F_{R-\text{in},CH_4}$ is the methane flowrate at the inlet of CLR Reactor, t_0 and t_f are the initial time and final time of integration, with $t_f = \tau_{OX} + \tau_{RED} + \tau_{REF}$.

$$\phi = \left[\boldsymbol{u}_i, \tau_{OX}, \tau_{RED}, \tau_{REF}, \omega, F_{S-\text{in},H_2O}\right] \in \boldsymbol{\Phi}. \quad (3)$$

$$\eta = \frac{\int_{t_0}^{\tau_{REF}} F_{S-\text{out},H_2}(t)dt}{\int_{t_0}^{t_f} F_{R-\text{in},CH_4}(t)dt}, \quad (4)$$

The optimization of the integrated system is subject to the following constraints. A minimum methane conversion (X_{CH_4}) of 96% in the CLR reactor must be achieved during both RED and REF (Eq. (5)). During OX, the CLR reactor must yield a N_2 stream with 98% minimum mole fraction, as shown in Eq. (6), where $F_{R-\text{out},N_2}$ is the N_2 molar flowrate at the exit of CLR reactor and $F_{R-\text{out},T}$ is the total flowrate at the exit of CLR reactor. Since the product stream of the CLR reactor is used in the heat recovery system, the total enthalpy carried by the product stream must exceed the enthalpy required for gas preheating and steam generation, Eq. (7), where, $F_{R-\text{in},T}$ is the total flowrate at the inlet of the CLR reactor, c_p is the heat capacity of the inlet/oulet streams, h_{fg,H_2O} is the enthalpy of evaporation of water, $T_{R-\text{in}}$ and $T_{R-\text{out}}$ are the inlet and outlet temperatures at the CLR reactor, respectively. In Eq. (7), it is assumed that in the heat recovery system product streams are cooled to 200 °C, while feed streams are heated up from 25°C. $F_{R-\text{in},H_2O}$ and $F_{S-\text{in},H_2O}$ are the molar flowrate of steam fed into CLR reactor and Shift reactor, respectively. To prevent agglomeration and sintering of the Ni-based oxygen carrier, the maximum temperature allowed in CLR reactor, $T_{R-\text{bed}}$, at any axial location z, must not exceed 1100°C, (Eq. (8)). The preheater must be able to heat up the cold stream, $T_{PR-\text{c,out}}$, to between 500 and 700°C, the desired temperature for feed gas of the CLR reactor (Eq. (9)). In the steam

generator, the exit temperature of the hot stream, $T_{SG-h,out}$, must be between 200 and 250°C, close to the operation temperature of the Shift reactor as in Eq. (10).

The complete optimal control problem can be formulated as shown in Eq. (11), where $\mathbf{f}$ is the set of differential-algebraic equations (DAEs) that describe the model of the reactors in the integrated CLR-Shift system, comprising mass, energy, and momentum balance and reaction kinetics, $\mathbf{x}$ is the vector of state variables (*i.e.*, mass, temperature, and pressure), and $\dot{\mathbf{x}}$ is time derivatives of $\mathbf{x}$. Cyclic steady-state conditions are typically achieved after more than two cycles. Therefore, the optimization time horizon was set to at least two times the τ_{cycle}.

$$X_{\text{CH}_4}(t) = 1 - \frac{\int_{t_0}^{t_f} F_{R-\text{out},\text{CH}_4}(t)dt}{\int_{t_0}^{t_f} F_{R-\text{in},\text{CH}_4}(t)dt} \geq 96\%\,, \tag{5}$$

$$\beta(t) = \frac{\int_{t_0}^{\tau_{\text{OX}}} F_{R-\text{out},\text{N}_2}(t)dt}{\int_{t_0}^{\tau_{\text{OX}}} F_{R-\text{out},T}(t)dt} \geq 98\%\,, \tag{6}$$

$$\begin{aligned}\gamma(t) = {} & \int_{t_0}^{t_f} F_{R-\text{out},T}(t)c_{p,\text{out}}(T_{R-\text{out}}(t) - 200\text{°C})dt \\ & - \int_{t_0}^{t_f} F_{R-\text{in},T}(t)c_{p,\text{in}}(T_{R-\text{in}}(t) - 25\text{°C})dt \\ & - \int_{t_0}^{\tau_{\text{REF}}} \left(F_{R-\text{in},\text{H}_2\text{O}}(t) + F_{\text{S}-\text{in},\text{H}_2\text{O}}(t)\right) h_{fg,\text{H}_2\text{O}}dt \geq 0,\end{aligned} \tag{7}$$

$$T_{R-\text{bed}}(z) \leq 1100\text{°C}\,, \tag{8}$$

$$500\text{°C} \leq T_{PR-\text{c,out}}(t) \leq 700\text{°C}\,, \tag{9}$$

$$200\text{°C} \leq T_{SG-\text{h,out}}(t) \leq 250\text{°C}\,, \tag{10}$$

$$\begin{aligned}&\max_{\phi\in\boldsymbol{\phi}} \eta \\ &\text{subject to:} \\ &\mathbf{f}(\dot{\mathbf{x}}(t), \mathbf{x}(t), \mathbf{u}(t), \boldsymbol{\theta}, t) = 0, \\ &\mathbf{f_0}(\dot{\mathbf{x}}(t_0), \mathbf{x}(t_0), \mathbf{u}(t_0), \boldsymbol{\theta}, t_0) = 0, \\ &\text{Eqs. } (5) - (10), \\ &\mathbf{x}^{\mathbf{min}} \leq \mathbf{x}(t) \leq \mathbf{x}^{\mathbf{max}}, \\ &\mathbf{u}_i{}^{\mathbf{min}} \leq \mathbf{u}_i(t) \leq \mathbf{u}_i{}^{\mathbf{max}}, \\ &\boldsymbol{\tau}_i{}^{\mathbf{min}} \leq \boldsymbol{\tau}_i(t) \leq \boldsymbol{\tau}_i{}^{\mathbf{max}}, \\ &\omega^{\mathbf{min}} \leq \omega \leq \omega^{\mathbf{max}}.\end{aligned} \tag{11}$$

The system of DAEs were built and solved in the equation-based process modeling platform gPROMS Model Builder, 7.0.9 [13]. For the spatial discretization, the backward finite difference method was used, dividing the reactor's axial direction into 21 nodes and its solid particle radial direction into 11 nodes. The system of DAEs was then solved with the DAEBDF solver. The non-linear optimization was solved with control vector parameterization with single shooting (CVP_SS) solver available in gPROMS. With control vector parameterization, the control variables were discretized as piecewise constant over a specified time interval, while with the single shooting approach, the control variables were fixed during the entire respective time horizon in each iteration.

RESULTS AND DISCUSSION

The integrated CLR-Shift system was used to study its performance for small-scale blue hydrogen and nitrogen production. The system was configured to run in parallel with multiple CLR reactors, collectively achieving a production rate of 300 kg-H_2 per day. **Table 4** (top rows) reports the reactor design and operating parameters, including reactor diameter, length, and operating pressure. Eq. (11) was solved, resulting in the optimized control variables reported in **Table 4** (bottom rows). These parameters were then used in simulations to evaluate the performance of the integrated CLR-Shift system.

Table 4: Parameters used in the integrated CLR-Shift system. The top rows are the common parameters, while the bottom rows show the optimized parameters.

Parameters	Values		
	OX	RED	REF
CLR Reactor			
- length, [m]		1.5	
- diameter, [m]		0.6	
Shift Reactor			
- length, [m]		0.6	
- diameter, [m]		0.6	
Operating pressure, [bar]		1.5	
Feed vol. flow, [NCMH]	360	36	180
CO_2-to-CH_4 ratio	--	4.0	--
Steam-to-CH_4 ratio	--	--	1.5
Feed temp., [°C]	600	600	600
CLR stages interval, [s]	150	135	200
Active metal in OC, [%]		5	
Add. steam @ Shift, [mol/s]	--	--	0.81

Figure 4 presents the exit mole fractions of CLR and Shift reactors at cyclic steady state. At the optimal operating conditions, the exit stream of the CLR reactor (**Figure 4a**) exhibits compositions of 98% N_2 during OX, 70% CO_2 and 30% steam during RED, and 66% H_2 during REF. The N_2 stream with high purity during OX is promising for the further integration with an ammonia plant. In RED, the exit stream, consist of CO_2 and H_2O, can be separated by a condensing unit before captured or recirculated for plant utility. The 66% H_2 during REF showcases the feasibility of CLR as one promising route for blue hydrogen production. In REF, there is also smaller gas constituents consisting of CO (20%), H_2O (10%), and CO_2 (2%) that need further purification.

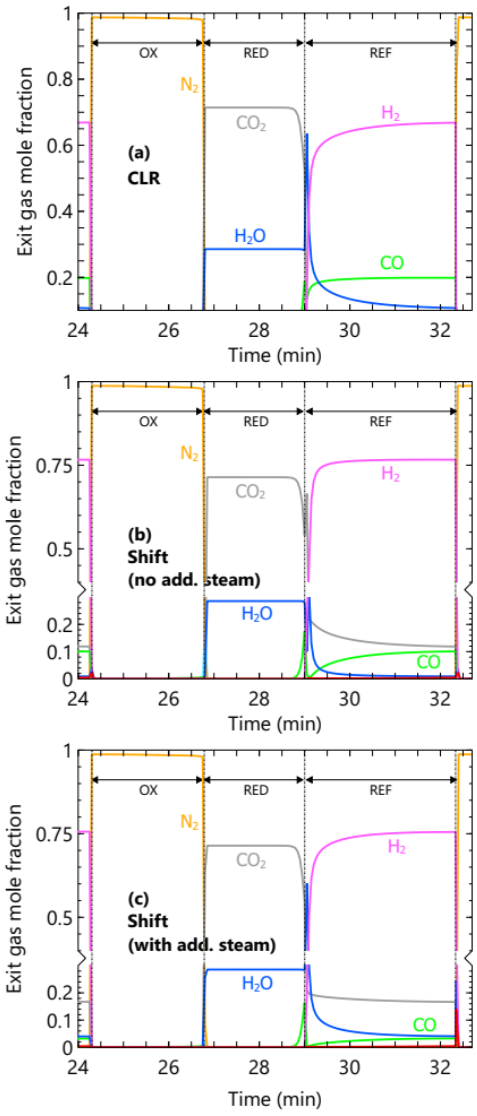

Figure 4. The performance of CLR and Shift reactor during cyclic steady-state, simulated at optimized parameters (Table 4). (a) Exit mole fraction at CLR Reactor; (b) exit mole fraction at Shift reactor without additional steam (Case 1); and (c) exit mole fraction at Shift reactor with additional steam (Case 2).

The product stream from CLR goes to the heat recovery system and serves as a heat source. **Figure 5** shows the temperature of the CLR product stream decreasing as it passes through the preheater and the steam generator, respectively. From the CLR reactor, the temperature of product stream is around 950°C. As the product stream exits the preheater, the temperature drops to 300–500°C. The exit temperature at the preheater varies in each CLR stage depending on the enthalpy remaining and temperature difference between hot and cold streams. Nonetheless, the CLR feed gas is successfully preheated to 500–700°C. The product stream then enters the steam generator producing steam needed for the reforming reactions. The steam generator operates in each CLR stage, using the remaining available enthalpy and temperature in the product stream as a heat source. The portion of the steam generated in each stage was tuned so that the exit temperature of the product stream in the steam generator was close to 200 °C (**Figure 5**).

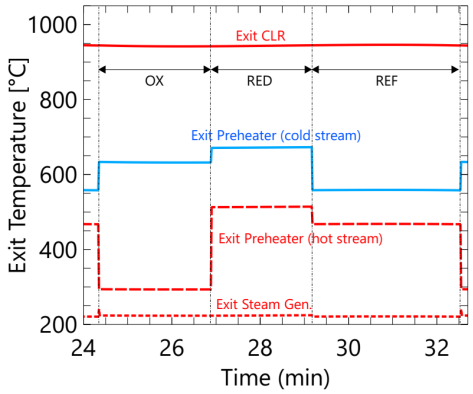

Figure 5. Exit gas temperature in the preheating and steam generating systems. The exit stream of CLR reactor is used as the heat source for the preheating and steam generating systems. The exit preheater cold stream feeds the CLR, while the hot stream from the preheater is used for steam generation.

We explored two scenarios for the Shift reactor: 1) Shift reactor without additional steam (Case 1), and 2) Shift reactor with additional steam (Case 2). In Case 1, the feed of the Shift reactor is the CLR product stream that has been cooled in the heat recovery system. In Case 2, an optimized amount of steam (**Table 4**) is added to the feed during REF. **Figures 4b** and **4c** present the result of Case 1 and Case 2, respectively. In both cases, the Shift reactor increased H_2 mole fraction from 66% to 75-76%. In Case 1, CO conversion was low, only 49.2%, due to the limited steam available for water gas shift reaction. At the exit, around 10% of CO remain unconverted and the H_2 production rate was 3 mol/s. In Case 2, the steam addition increased the extent of the water gas shift reaction and increased CO conversion to 82.7%. At the exit, H_2 production rate was 3.2 mol/s (75.6% of the total stream), with smaller gas constituents consisting of: CO_2 (16.7%), H_2O (4%), and CO (3.2%).

Overall, the integrated CLR-Shift reactors system successfully generated H_2 and N_2, with high concentration and efficiency. In Case 1, H_2 and N_2 were produced with a ratio of 1.16 and an H_2 production efficiency of 74.9%. Meanwhile, Case 2 yielded H_2 and N_2 with a ratio of 1.26 and an H_2 production efficiency of 80.1%. Furthermore, the dynamic operation of this integrated system suggest the possibility of integration with an ammonia synthesis process reported in [14].

CONCLUSIONS

Integration of the CLR reactor, Shift reactor, and heat recovery system demonstrated promising results for blue hydrogen and nitrogen production. An optimized control scheme is crucial to ensure high H_2 production that satisfies the numerous system constraints. Under the optimized control scenario, the integrated CLR-Shift reactors system produced H_2 with a 75% mole fraction during REF, N_2 with 98% purity during OX, and a potential for CO_2 capture during RED. The control scenario is also essential in distributing the heat within the integrated system, meeting the heat requirements for overall reactions, the feed gas preheating and steam generation. The addition of steam in the Shift reactor is essential to maintain steam availability for the water gas shift reaction. Further purification in the downstream product, such as pressure-swing adsorption, must be considered to achieve higher H_2 purity. A future study on multiple reforming reactor system and reactor scheduling will target a continuous flow of hydrogen and nitrogen products.

ACKNOWLEDGEMENTS

This work was supported by a DIKTI-funded Fulbright Fellowship and the Pratt & Whitney Institute of Advanced Systems Engineering (P&W-IASE) of the University of Connecticut. Any opinions expressed herein are those of the author and do not represent those of the sponsor.

REFERENCES

1. IEA, “Towards hydrogen definitions based on their emissions intensity,” 2023. [Online]. Available: www.iea.org.
2. J. F. George, V. P. Müller, J. Winkler, and M. Ragwitz, “Is blue hydrogen a bridging technology? - The limits of a CO2 price and the role of state-induced price components for green hydrogen production in Germany,” *Energy Policy*, vol. 167, Aug. 2022, doi: 10.1016/j.enpol.2022.113072.
3. J. Andersson and S. Grönkvist, “Large-scale storage of hydrogen,” *Int. J. Hydrogen Energy*, vol. 44, no. 23, pp. 11901–11919, 2019, doi: 10.1016/j.ijhydene.2019.03.063.
4. C. A. Del Pozo, S. Cloete, Á. J. Álvaro, F. Donat, and S. Amini, “The potential of gas switching partial oxidation using advanced oxygen carriers for efficient h2 production with inherent co2 capture,” *Appl. Sci.*, vol. 11, no. 10, May 2021, doi: 10.3390/app11104713.
5. A. R. Irhamna and G. M. Bollas, “Process intensification in a fixed bed reactor for a small-scale process in the stranded assets,” in *33rd European Symposium on Computer Aided Process Engineering*, 2023, pp. 3043–3048.
6. Z. Zhou, L. Han, and G. M. Bollas, “Model-based analysis of bench-scale fixed-bed units for chemical-looping combustion,” *Chem. Eng. J.*, vol. 233, pp. 331–348, 2013, doi: 10.1016/j.cej.2013.08.025.
7. Z. Zhou, L. Han, O. Nordness, and G. M. Bollas, “Continuous regime of chemical-looping combustion (CLC) and chemical-looping with oxygen uncoupling (CLOU) reactivity of CuO oxygen carriers,” *Appl. Catal. B Environ.*, vol. 166–167, pp. 132–144, 2015, doi: 10.1016/j.apcatb.2014.10.067.
8. O. Nordness, L. Han, Z. Zhou, and G. M. Bollas, “High-Pressure Chemical-Looping of Methane and Synthesis Gas with Ni and Cu Oxygen Carriers,” *Energy and Fuels*, vol. 30, no. 1, pp. 504–514, 2016, doi: 10.1021/acs.energyfuels.5b01986.
9. A. R. Irhamna and G. M. Bollas, “Intensified reactor for lean methane emissions treatment,” *AIChE J.*, pp. 1–40, 2023, doi: 10.1002/aic.18040.
10. T. A. Adams and P. I. Barton, “A dynamic two-dimensional heterogeneous model for water gas shift reactors,” *Int. J. Hydrogen Energy*, vol. 34, no. 21, pp. 8877–8891, 2009, doi: 10.1016/j.ijhydene.2009.08.045.
11. Y. Choi and H. G. Stenger, “Water gas shift reaction kinetics and reactor modeling for fuel cell grade hydrogen,” *J. Power Sources*, vol. 124, no. 2, pp. 432–439, 2003, doi: 10.1016/S0378-7753(03)00614-1.
12. P. Alexandros Argyris *et al.*, “Chemical looping reforming for syngas generation at real process conditions in packed bed reactors: An experimental demonstration,” *Chem. Eng. J.*, vol. 435, May 2022, doi: 10.1016/j.cej.2022.134883.
13. Process Systems Enterprise, “gPROMS.” 2021, [Online]. Available: www.psenterprise.com/products/gproms.
14. L. Burrows, P. X. Gao, and G. M. Bollas, “Thermodynamic feasibility analysis of distributed chemical looping ammonia synthesis,” *Chem. Eng. J.*, vol. 426, no. May, p. 131421, 2021, doi: 10.1016/j.cej.2021.131421.